Deep learning analysis of mid-infrared microscopic imaging data for the diagnosis and classification of human lymphomas

Philipp Zelger[1], Andrea Brunner[1], Bettina Zelger[1], Ella Willenbacher[2], Seraphin Unterberger[3], Roland Stalder[3], Christian Huck[4], Wolfgang Willenbacher[2], and Johannes Pallua[1]

[1]Medical University of Innsbruck
[2]Medizinische Universität Innsbruck
[3]Leopold Franzens Universität für Innsbruck
[4]Affiliation not available

January 20, 2023

Abstract

The present study presents an alternative analytical workflow that combines mid-infrared (MIR) microscopic imaging and deep learning to diagnose human lymphoma and differentiate between small and large cell lymphoma. We could show that using a deep learning approach to analyze MIR hyperspectral data obtained from benign and malignant lymph node pathology results in high accuracy for correct classification, learning the distinct region of 3900 cm-1 to 850 cm-1. The accuracy is above 95% for every pair of malignant lymphoid tissue and still above 90% for the distinction between benign and malignant lymphoid tissue for binary classification. These results demonstrate that a preliminary diagnosis and subtyping of human lymphoma could be streamlined by applying a deep learning approach to analyze MIR spectroscopic data.

Deep learning analysis of mid-infrared microscopic imaging data for the diagnosis and classification of human lymphomas

Short title: Deep learning analysis of Mid-infrared microscopic human lymphomas imaging data

P. Zelger[1][*], A. Brunner[2][*] , B. Zelger[2], E. Willenbacher[3], S. H. Unterberger[4], R. Stalder[5], C. W. Huck[6], W. Willenbacher[3,7], J. D. Pallua[8][#]

[1]*University Hospital of Hearing, Voice and Speech Disorders, Medical University of Innsbruck, Anichstrasse 35, 6020 Innsbruck, Austria*

[2]*Institute of Pathology, Neuropathology and Molecular Pathology, Medical University of Innsbruck, Müllerstraße 44, 6020 Innsbruck, Austria*

[3]*University Hospital of Internal Medicine V, Hematology & Oncology, Medical University of Innsbruck, Anichstrasse 35,6020 Innsbruck, Austria*

[4]*Institute of Material-Technology, Leopold-Franzens University Innsbruck, Technikerstraße 13, 6020 Innsbruck, Austria*

[5]*Institute of Mineralogy and Petrography, Leopold-Franzens University Innsbruck, Innrain 52 6020 Innsbruck, Austria*

[6]*Institute of Analytical Chemistry and Radiochemistry, Innrain 80-82, 6020 Innsbruck, Austria*

*7*Oncotyrol, Centre for Personalized Cancer Medicine, Karl-Kapferer-Straße 5, 6020 Innsbruck, Austria

*8*University Hospital for Orthopaedics and Traumatology, Medical University of Innsbruck, Anichstraße 35, 6020 Innsbruck, Austria

*both authors contributed equally

#Corresponding author:

Priv.-Doz. MMag. Dr. Johannes Dominikus Pallua MSc PhD

University Hospital for Orthopedics and Traumatology,

Medical University of Innsbruck,

Anichstraße 35, 6020 Innsbruck, Austria

Mail: Johannes.Pallua@i-med.ac.at

Abstract

The present study presents an alternative analytical workflow that combines mid-infrared (MIR) microscopic imaging and deep learning to diagnose human lymphoma and differentiate between small and large cell lymphoma. We could show that using a deep learning approach to analyze MIR hyperspectral data obtained from benign and malignant lymph node pathology results in high accuracy for correct classification, learning the distinct region of 3900 cm^{-1} to 850 cm^{-1}. The accuracy is above 95% for every pair of malignant lymphoid tissue and still above 90% for the distinction between benign and malignant lymphoid tissue for binary classification. These results demonstrate that a preliminary diagnosis and subtyping of human lymphoma could be streamlined by applying a deep learning approach to analyze MIR spectroscopic data.

Keywords: deep learning, mid-infrared microscopic imaging, diffuse large B-cell-lymphoma, follicular lymphoma

Abbreviation:

ANN: neural network

CAE: Convolutional Autoencoder

DA: discriminant analysis

DLBCL: diffuse large B-cell lymphoma

FC: follicle centre

FL: follicular lymphoma

GCB: germinal centre

HCA: hierarchical cluster analysis

MIR: Mid-infrared

MZ: mantle zone

non-GCB: non-germinal centre

PCA: principal component analysis

PLS: partial least squares

RF: random forest

rLN: Reactive (normal) lymph nodes

SVMs: support vector machines

Introduction

Mid-infrared (MIR) microscopic imaging is a modern analytical method that is widely used to characterize the components of biological specimens [1-3] and has already been applied in tissue histology [4-6]. MIR microscopic imaging was, for example, used to aid in the differentiation between benign and malignant disease [3, 5, 7-11] and was tested for imaging lymph node histopathology [6, 12]. Our group successfully implemented this method for the differentiation between reactive lymph nodes, small and large cell lymphoma using follicular lymphoma (FL), and diffuse large B-cell lymphoma (DLBCL) as an example [13].

IR microscopic imaging experiments are measurements that include high-quality and high-quantity information. Thus, chemometric tools in imaging analysis are a prerequisite to taking advantage of the entire measurement [14]. Statistical classification methods have been used for histopathological studies, which discriminate between pixels of healthy tissue versus pixels of diseased tissue [15, 16]. Multifactorial statistical analysis methods related to IR data have been widely implemented for identifying changes in lipids, proteins, nucleic acids, and carbohydrates, such as principal component analysis (PCA) [17, 18] and partial least squares (PLS) [19, 20] combined with discriminant analysis (DA) [21], hierarchical cluster analysis (HCA) [22], support vector machines (SVMs) [23] and random forest (RF) [24]. As a pattern-recognition-based approach, the (artificial) neural network ((A)NN) proved to be effective in analyzing data obtained from biological specimens, also using IR imaging techniques [25-27]. NNs perform best when trained with a large amount of labelled data [28, 29]. However, in pathology, labelling data, which means (whole-slide) images, is complex and time-consuming [28]. These limitations can be eliminated by employing so-called self-supervised and unsupervised techniques [28, 29]. One unsupervised technique is the Convolutional Autoencoder (CAE), which is trained with unlabelled data [29, 30]. Such NNs were developed to work with high-dimensional data and have already been implemented to solve medical problems, such as radiology, cardiology, neurology, and even pathology [30-34]. In brief, the input layer of the CAE compresses the data and creates a code, which is then used to reconstruct them in the output layer [30]. The CAE-based network consists of several convolutional layers with a decreasing number of filters that create a bottleneck in the centre of the network (**Figure 1a**). After this bottleneck, the number of neurons increases again, allowing the network to reproduce the input data. The bottleneck in the centre of the CAE forces the NN to learn the features of the input data. This can be compared to a dimensionality reduction as performed with PCA [30].

This study combines MIR imaging of unstained tissue slides and a deep learning approach using CAE as an example of an unsupervised technique to differentiate between benign and malignant lymphoid tissues and to classify lymphoma subtypes.

Materials and Methods

Patients and Material

The dataset acquired as part of our previous study on MIR imaging of human lymphomas was used [13]. This dataset includes MIR measurements of six cases of FL and 12 cases of DLBCL (five germinal centre (GCB) and seven non-germinal centre (non-GCB) subtypes), which were diagnosed between 2002 and 2012 at the Institute of Pathology, Neuropathology, and Molecular Pathology, Medical University of Innsbruck. Reactive (normal) lymph nodes (rLN) served as control. The study was conducted according to the IHC-GCP guidelines and the declaration of Helsinki. Ethical approval was obtained from the ethical committee of the Medical University of Innsbruck (EK-Nr.1213/2017). For information on initial sample preparation and MIR imaging, please refer to Willenbacher E et al. (2021) [13].

Data Processing

In order to classify data by a neural network, the network has to learn a feature representation of the data. Usually, this is achieved by training on a big set of labelled data. Labelling histological data, however, is time-consuming and expensive. A solution to that issue is to train the network in an unsupervised manner. To do so we implemented a convolutional autoencoder (CAE). Those neural networks have a bottleneck in

their architecture. This bottleneck forces the network to learn a reduced representation of the data. This reduced representation can then be used as input for a classifier network.

We fed the single-pixel spectra of the two-dimensional dataset into the ANN. A total number of over 1 million single spectra from different IR datasets was used to pre-train the CAE. Using a large variety of data allows the neural network to learn the features of the IR data without the danger of overfitting the network [29].

The neural network was implemented using Python and Tensorflow. The training of the Autoencoder took around 4 hours on an NVidia GTX 1080 GPU. After this network preparation, the so-called decoder part (blue layers in **Figure 1a**) of the Autoencoder has been removed. The updated neural network ends at the bottleneck. All the layers are frozen at this point, which means they cannot be altered anymore by further training. With that, the previous feature extraction capabilities are preserved. Next, a small neural network consisting of two layers with ten fully connected neurons is added to the network. These two layers are connected to the output of the network, which, depending on the task, consists of several (for multiclass classification) or one (for binary classification) output neurons (**Figure 1b**).
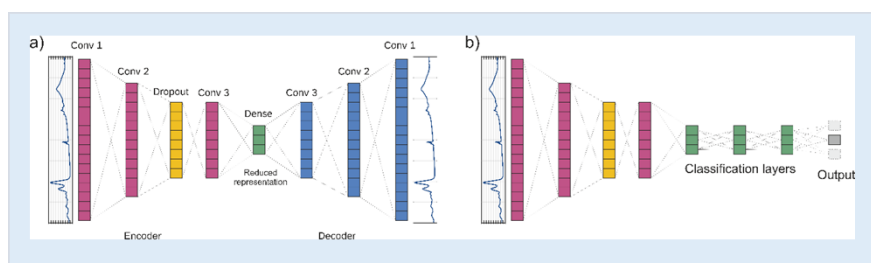

Figure 1. a) Schematic of the CAE. The CAE receives an IR spectrum as input and tries to reproduce this input data. The pink convolutional layers have a Kernel size of 10 with 32,64, and 32 filters. An additional Dropout layer (20% dropout rate) was added to prevent overfitting. The green layer describes a fully connected dense layer with 24 neurons. The blue part of the network consists of three upscaling convolutional layers with a kernel size of 3,5 and 4, respectively, and 64,128 and 55 Filters. The total number of parameters accounts for 800.863 parameters. **b)** The green layers represent the two added dense layers with 10 neurons for the classification tasks. The grey squares represent output neurons. The number of output neurons depends on the number of classes to be distinguished. The trainable parameters account for 261.

This final part of the network will be trained to classify the different subtypes of lymphoma and normal (reactive) control. It uses the pre-trained feature detection of the first part of the Autoencoder. With that, the number of parameters to be fitted is reduced to 253 Parameters.

Labelling training and test data are required to train the classifier part of the neural network. Here, areas of interest in lymphoma tissue (FL = follicular and intrafollicular area; DLBCL, non-GCB and DLBCL, GCB subtype) and rLN were labelled, and the corresponding spectra were extracted. One sample served as a training set, and the other as an evaluation set. The labelling procedure of the training data is depicted in **Figure 2** .
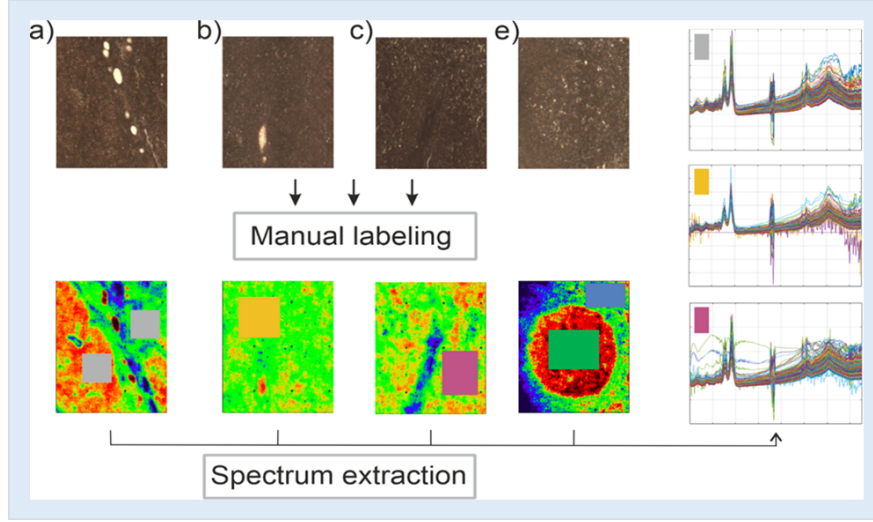
Figure 2 Workflow for the labelling and extraction of the training and evaluation spectra of the different classes. The first row shows the optical images of the FL (a), DLBCL (b and c), and normal control (e). The second row shows the labelled regions. The coloured labels correspond to FL (grey), DLBCL, non-GCB subtype (orange), DLBCL, GCB subtype (pink), and rLNs (green = follicle centre (FC); blue = mantle zone (MZ)). The right column shows a selection of spectra, with the type corresponding to the coloured bar on the left.

Table 1 shows the type of disease, label colour as manually assigned (see figure 2), and the number of spectra obtained for analysis.

Type	FL	DLBCL, non-GCB	DLBCL, GCB	rLN$^{\text{FC}}$	rLN$^{\text{MZ}}$
Colour in Fig. 2	Grey	Orange	Pink	Green	Blue
Nr. Spectra	45.000	40.000	50.000	35.000	45.000

Table 1. Type of tissue, the colour of label and number of spectra obtained for this study

After labelling, the following steps were carried out:

Application of the network to distinguish between benign and malignant lymphoid tissue types. To do so, the neural network is trained with two sets of spectral data (e.g., FL vs DLBCL, non-GCB). The evaluation of the deep classifier is done on the second set of spectra containing the respective classes.

Classification of more than two types (multiclass) of neoplastic and reactive lymphoid tissue.

Results

Figure 3 shows the binary (left side) and multiclass (right side) classification obtained from MIR imaging data applying the deep learning approach described above.
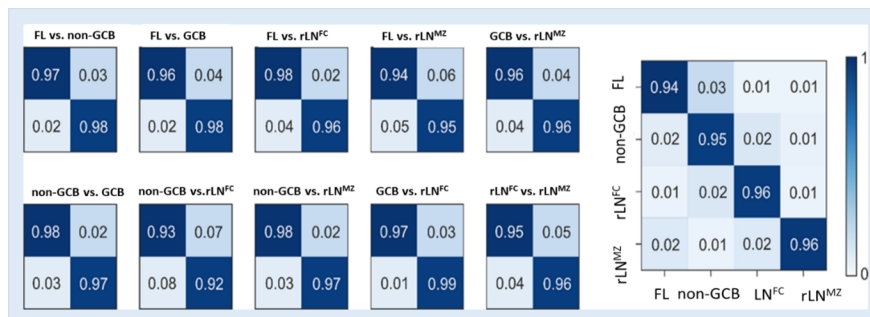
Figure 3 Confusion matrices for the binary (right side) and multiclass (left side) classification between the benign and malignant lymphoid tissues. The x-axis shows the true label. The y-axis corresponds to the predicted label.

As shown in **Figure 3,** the accuracy is above 95% for every pair of malignant lymphoid tissue and still above 90% for the distinction between benign and malignant lymphoid tissue. The multiclass classification between the lymphoma types (FL and DLBCL) and rLN^{FC} and rLN^{MZ} leads to similarly high accuracy for the binary classification. This multiclass classification's accuracy is still above 94 % for all neoplastic and reactive lymphoid tissue types.

The neural network, once trained, performs a forward execution of a complex function depicted by the NN, representing the analysis of an IR image in less than 25 ms. NNs with three output classes have been trained to visualize the capabilities of the deep learning approach. These three classes serve as a colour code for an RGB image, whereby the NN classifies the spectrum of each pixel. This means that it was decided to which class the corresponding subsection belongs for each pixel individually. This leads to the satisfactory resolution images shown in**Figure 4 A-C** .
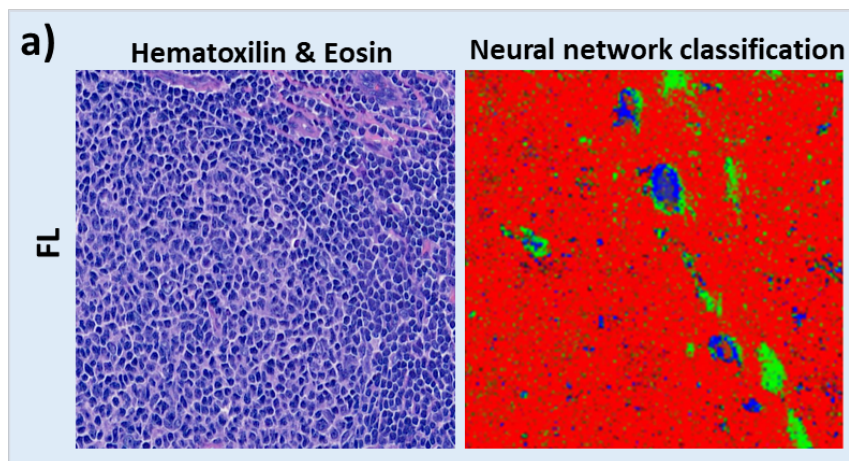

Figure 4 a) Results of the classification of the NN for FL showing histology on the left side and the right side neural network classification with FL (follicular/intrafollicular) in red, GCB in green and normal tissue (rLN^{FC}) in blue.
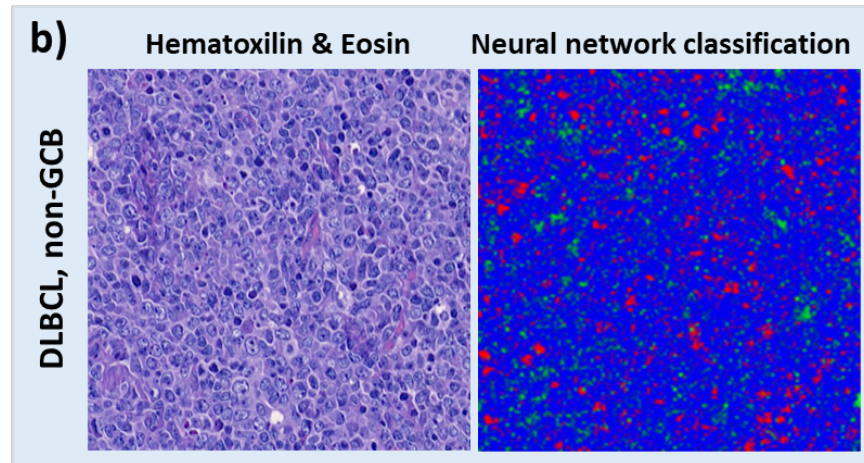
6

Figure 4 b) Results of the classification of the NN for DLBCL, non-GCB showing histology on the left side and on the right side neural network classification with DLBCL, non-GCB in blue, GCB in green and normal tissue (rLN^{FC}) in red.
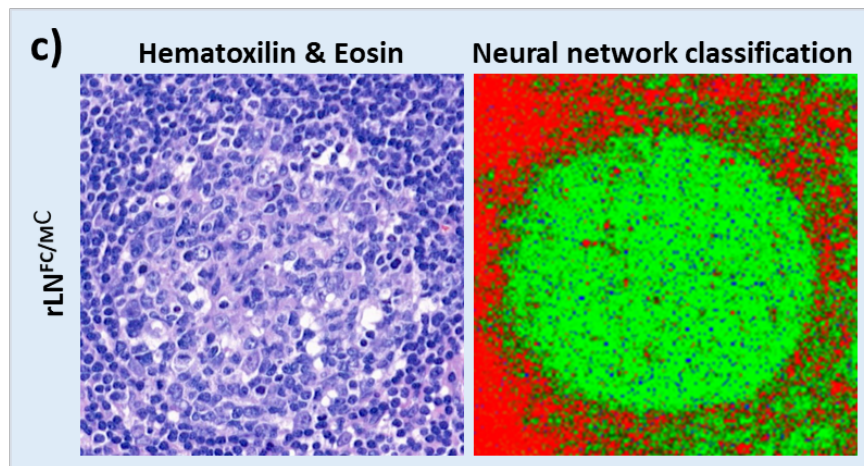

Figure 4 c) Results of the classification of the NN for rLN$^{FC/MZ}$ showing histology on the left side and the right side neural network classification with rLN^{FC} in green and rLN^{MZ} in red and FL in blue.

Discussion

Our study showed that using a deep learning approach to analyze MIR imaging data from unstained histological slides can distinguish between benign and malignant lymphoid tissue and aid in classifying types of lymphomas. MIR imaging on tissue sections results in large and complex data sets that must be analyzed and interpreted. Focussing on possible use in routine diagnostics, the data acquisition and the subsequent analysis must take place within a narrow time window to offer an advantage over standard pathological diagnostics or assist the pathologist during the diagnostic procedure. A deep learning approach using NNs, offers such a possibility. Our NN, once trained, analyzed a MIR image in less than 25 ms. However, training NNs using a deep learning approach takes considerable time and requires graphical processing units (GPUs) and high-performance machines to process digital images [28, 30]. The training, however has to be performed only once, and the NN can then be used to classify IR data without further training. This even allows for real-time spectrum analysis.

7

NNs have already been implemented in medicine and used in various studies in the fields of radiology, cardiology, neurology, and pathology [30-34]. But several caveats prevent such techniques from being widely used. One of the most important is undoubtedly the "black box" character of such analyses [29, 30]. The decisions of such algorithms are not easy for the human user to understand and interpret. Therefore, a certain scepticism about such approaches is understandable, especially in medicine, where comprehensible decisions with sometimes severe consequences for patients must be made and justified [28, 29].

Another problem is the need for large datasets to train NNs for a specific problem [28, 30]. Small datasets result in poor performance of NNs, while on the other hand, one has to bear in mind not to "overfit" a NN [29, 30]. In the case of pathological diagnoses, obtaining such datasets is a significant problem, especially regarding rare diseases. But one has also to consider the extreme variability of histopathological patterns derived from various tissue types, building up organs [28]. Additionally, data quality is essential, especially when dealing with pixel-based data (images) in pathology, where artefacts might pose serious problems [28, 35, 36]. In fact, concerning MIR imaging, there are currently no available datasets that could be used, and it is also questionable if there will be any in the future. Overall, it is doubtful that any deep learning approach using NNs, combined with MIR microscopic imaging, will replace pathologists in the foreseeable future. It is more likely, that deep learning-driven approaches will be used to assist a pathologist during the diagnostic procedure [37].

Finally, besides technical questions and dataset availability, ethical and legal questions are also associated with the use of deep learning in decision-making processes in pathology. These fundamental questions range from concern about data privacy to the question of responsibility for a wrong decision based on a deep learning approach [29]. However, when there are fewer and fewer pathologists, deep learning techniques may assist as a diagnostic tool to support the pathologist in stratifying patients, identifying urgent cases, and thus better directing the routine workflow.

Finally, the financial side of introducing such technologies must also be considered. The financial pressure on pathology laboratories is already a challenge because of the increasing digitization and subsequent data storage [28]. The acquisition of access to the appropriate hard- and software, such as GPU clusters, as a must to train deep learning algorithms in practice, could fail due to a lack of funding [28, 38].

Our results demonstrate that a diagnosis and subtyping of human lymphoma could be streamlined based on MIR microscopy and a deep learning approach for data analysis. This might be a complementary pathway for a quick preliminary assessment of the type and aggressiveness of the disease and could probably help in advance to identify urgent diagnoses and, given the increasing shortage of pathologists, to prioritize these patients in the routine workflow.

Acknowledgements

References

[1] S. Turker-Kaya, C.W. Huck, A Review of Mid-Infrared and Near-Infrared Imaging: Principles, Concepts and Applications in Plant Tissue Analysis, Molecules 22 (2017).

[2] E. Kontsek, A. Pesti, M. Bjornstedt, T. Uveges, E. Szabo, T. Garay, P. Gordon, S. Gergely, A. Kiss, Mid-Infrared Imaging Is Able to Characterize and Separate Cancer Cell Lines, Pathol Oncol Res 26 (2020) 2401-2407.

[3] S. Mittal, R. Bhargava, A comparison of mid-infrared spectral regions on accuracy of tissue classification, Analyst 144 (2019) 2635-2642.

[4] J. Nallala, G.R. Lloyd, N. Shepherd, N. Stone, High-resolution FTIR imaging of colon tissues for elucidation of individual cellular and histopathological features, Analyst 141 (2016) 630-639.

[5] J.A. Kimber, L. Foreman, B. Turner, P. Rich, S.G. Kazarian, FTIR spectroscopic imaging and mapping with correcting lenses for studies of biological cells and tissues, Faraday Discuss 187 (2016) 69-85.

[6] L.S. Leslie, T.P. Wrobel, D. Mayerich, S. Bindra, R. Emmadi, R. Bhargava, High definition infrared spectroscopic imaging for lymph node histopathology, PLoS One 10 (2015) e0127238.

[7] H. Sreedhar, V.K. Varma, P.L. Nguyen, B. Davidson, S. Akkina, G. Guzman, S. Setty, A. Kajdacsy-Balla, M.J. Walsh, High-definition Fourier Transform Infrared (FT-IR) spectroscopic imaging of human tissue sections towards improving pathology, J Vis Exp (2015) 52332.

[8] C.H. Petter, N. Heigl, M. Rainer, R. Bakry, J. Pallua, G.K. Bonn, C.W. Huck, Development and application of Fourier-transform infrared chemical imaging of tumour in human tissue, Curr Med Chem 16 (2009) 318-326.

[9] J.D. Pallua, C. Pezzei, B. Zelger, G. Schaefer, L.K. Bittner, V.A. Huck-Pezzei, S.A. Schoenbichler, H. Hahn, A. Kloss-Brandstaetter, F. Kloss, G.K. Bonn, C.W. Huck, Fourier transform infrared imaging analysis in discrimination studies of squamous cell carcinoma, Analyst 137 (2012) 3965-3974.

[10] C. Pezzei, J.D. Pallua, G. Schaefer, C. Seifarth, V. Huck-Pezzei, L.K. Bittner, H. Klocker, G. Bartsch, G.K. Bonn, C.W. Huck, Characterization of normal and malignant prostate tissue by Fourier transform infrared microspectroscopy, Mol Biosyst 6 (2010) 2287-2295.

[11] J. Laimer, R. Henn, T. Helten, S. Sprung, B. Zelger, B. Zelger, R. Steiner, D. Schnabl, V. Offermanns, E. Bruckmoser, C.W. Huck, Amalgam tattoo versus melanocytic neoplasm - Differential diagnosis of dark pigmented oral mucosa lesions using infrared spectroscopy, PLoS One 13 (2018) e0207026.

[12] M. Isabelle, K. Rogers, N. Stone, Correlation mapping: rapid method for identification of histological features and pathological classification in mid infrared spectroscopic images of lymph nodes, J Biomed Opt 15 (2010) 026030.

[13] E. Willenbacher, A. Brunner, B. Zelger, S.H. Unterberger, R. Stalder, C.W. Huck, W. Willenbacher, J.D. Pallua, Application of mid-infrared microscopic imaging for the diagnosis and classification of human lymphomas, J Biophotonics 14 (2021) e202100079.

[14] M.J. Baker, J. Trevisan, P. Bassan, R. Bhargava, H.J. Butler, K.M. Dorling, P.R. Fielden, S.W. Fogarty, N.J. Fullwood, K.A. Heys, C. Hughes, P. Lasch, P.L. Martin-Hirsch, B. Obinaju, G.D. Sockalingum, J. Sule-Suso, R.J. Strong, M.J. Walsh, B.R. Wood, P. Gardner, F.L. Martin, Using Fourier transform IR spectroscopy to analyze biological materials, Nat Protoc 9 (2014) 1771-1791.

[15] P. Lasch, W. Haensch, D. Naumann, M. Diem, Imaging of colorectal adenocarcinoma using FT-IR microspectroscopy and cluster analysis, Biochim Biophys Acta 1688 (2004) 176-186.

[16] D.C. Fernandez, R. Bhargava, S.M. Hewitt, I.W. Levin, Infrared spectroscopic imaging for histopathologic recognition, Nat Biotechnol 23 (2005) 469-474.

[17] R.S. Uysal, I.H. Boyaci, Authentication of liquid egg composition using ATR-FTIR and NIR spectroscopy in combination with PCA, J Sci Food Agric 100 (2020) 855-862.

[18] A. Beljebbar, S. Dukic, N. Amharref, M. Manfait, Screening of biochemical/histological changes associated to C6 glioma tumor development by FTIR/PCA imaging, Analyst 135 (2010) 1090-1097.

[19] G.C. Andrade, C.M. Medeiros Coelho, V.G. Uarrota, Modelling the vigour of maize seeds submitted to artificial accelerated ageing based on ATR-FTIR data and chemometric tools (PCA, HCA and PLS-DA), Heliyon 6 (2020) e03477.

[20] P. Barmpalexis, A. Karagianni, I. Nikolakakis, K. Kachrimanis, Artificial neural networks (ANNs) and partial least squares (PLS) regression in the quantitative analysis of cocrystal formulations by Raman and ATR-FTIR spectroscopy, J Pharm Biomed Anal 158 (2018) 214-224.

[21] Y. Kou, Q. Li, X. Liu, R. Zhang, X. Yu, Efficient Detection of Edible Oils Adulterated with Used Frying Oils through PE-film-based FTIR Spectroscopy Combined with DA and PLS, J Oleo Sci 67 (2018) 1083-1089.

[22] D. Kong, W. Peng, R. Zong, G. Cui, X. Yu, Morphological and Biochemical Properties of Human Astrocytes, Microglia, Glioma, and Glioblastoma Cells Using Fourier Transform Infrared Spectroscopy, Med Sci Monit 26 (2020) e925754.

[23] Y. Li, F. Li, X. Yang, L. Guo, F. Huang, Z. Chen, X. Chen, S. Zheng, Quantitative analysis of glycated albumin in serum based on ATR-FTIR spectrum combined with SiPLS and SVM, Spectrochim Acta A Mol Biomol Spectrosc 201 (2018) 249-257.

[24] H.Z. Chen, G.Q. Tang, W. Ai, L.L. Xu, K. Cai, Use of random forest in FTIR analysis of LDL cholesterol and tri-glycerides for hyperlipidemia, Biotechnol Prog 31 (2015) 1693-1702.

[25] E. Kaznowska, J. Depciuch, K. Lach, M. Kolodziej, A. Koziorowska, J. Vongsvivut, I. Zawlik, M. Cholewa, J. Cebulski, The classification of lung cancers and their degree of malignancy by FTIR, PCA-LDA analysis, and a physics-based computational model, Talanta 186 (2018) 337-345.

[26] P. Lasch, M. Stammler, M. Zhang, M. Baranska, A. Bosch, K. Majzner, FT-IR Hyperspectral Imaging and Artificial Neural Network Analysis for Identification of Pathogenic Bacteria, Anal Chem 90 (2018) 8896-8904.

[27] S. Kimeswenger, P. Tschandl, P. Noack, M. Hofmarcher, E. Rumetshofer, H. Kindermann, R. Silye, S. Hochreiter, M. Kaltenbrunner, E. Guenova, G. Klambauer, W. Hoetzenecker, Artificial neural networks and pathologists recognize basal cell carcinomas based on different histological patterns, Mod Pathol 34 (2021) 895-903.

[28] H.R. Tizhoosh, L. Pantanowitz, Artificial Intelligence and Digital Pathology: Challenges and Opportunities, J Pathol Inform 9 (2018) 38.

[29] S.J. MacEachern, N.D. Forkert, Machine learning for precision medicine, Genome 64 (2021) 416-425.

[30] I.H. Sarker, Deep Learning: A Comprehensive Overview on Techniques, Taxonomy, Applications and Research Directions, SN Comput Sci 2 (2021) 420.

[31] S. Park, H.M. Gach, S. Kim, S.J. Lee, Y. Motai, Autoencoder-Inspired Convolutional Network-Based Super-Resolution Method in MRI, IEEE J Transl Eng Health Med 9 (2021) 1800113.

[32] J.H. Jang, T.Y. Kim, H.S. Lim, D. Yoon, Unsupervised feature learning for electrocardiogram data using the convolutional variational autoencoder, PLoS One 16 (2021) e0260612.

[33] H. Takahashi, A. Emami, T. Shinozaki, N. Kunii, T. Matsuo, K. Kawai, Convolutional neural network with autoencoder-assisted multiclass labelling for seizure detection based on scalp electroencephalography, Comput Biol Med 125 (2020) 104016.

[34] M. Roy, J. Kong, S. Kashyap, V.P. Pastore, F. Wang, K.C.L. Wong, V. Mukherjee, Convolutional autoencoder based model HistoCAE for segmentation of viable tumor regions in liver whole-slide images, Sci Rep 11 (2021) 139.

[35] V. Rastogi, N. Puri, S. Arora, G. Kaur, L. Yadav, R. Sharma, Artefacts: a diagnostic dilemma - a review, J Clin Diagn Res 7 (2013) 2408-2413.

[36] S. Chatterjee, Artefacts in histopathology, J Oral Maxillofac Pathol 18 (2014) S111-116.

[37] N. Grabe, W. Roth, S. Foersch, [Digital pathology in immuno-oncology-current opportunities and challenges : Overview of the analysis of immune cell infiltrates using whole slide imaging], Pathologe 39 (2018) 539-545.

[38] G. Andrade, R. Ferreira, G. Teodoro, L. Rocha, J.H. Saltz, T. Kurc, Efficient Execution of Microscopy Image Analysis on CPU, GPU, and MIC Equipped Cluster Systems, Proc Symp Comput Archit High Perform Comput 2014 (2014) 89-96.